Subscriber access provided by CORNELL UNIVERSITY LIBRARY

Article

Remarkable Structural Diversity between Zr/Hf and Rare-Earth MOFs via Ligand Functionalization and the Discovery of Unique (4, 8)-c and (4, 12)-connected Frameworks

Giasemi K. Angeli, Danai Batzavali, Katerina Mavronassou, Constantinos Tsangarakis, Tobias Stuerzer, Holger Ott, and Pantelis N. Trikalitis

J. Am. Chem. Soc., **Just Accepted Manuscript** • Publication Date (Web): 26 Aug 2020

Downloaded from pubs.acs.org on August 26, 2020

Just Accepted

“Just Accepted” manuscripts have been peer-reviewed and accepted for publication. They are posted online prior to technical editing, formatting for publication and author proofing. The American Chemical Society provides “Just Accepted” as a service to the research community to expedite the dissemination of scientific material as soon as possible after acceptance. “Just Accepted” manuscripts appear in full in PDF format accompanied by an HTML abstract. “Just Accepted” manuscripts have been fully peer reviewed, but should not be considered the official version of record. They are citable by the Digital Object Identifier (DOI®). “Just Accepted” is an optional service offered to authors. Therefore, the “Just Accepted” Web site may not include all articles that will be published in the journal. After a manuscript is technically edited and formatted, it will be removed from the “Just Accepted” Web site and published as an ASAP article. Note that technical editing may introduce minor changes to the manuscript text and/or graphics which could affect content, and all legal disclaimers and ethical guidelines that apply to the journal pertain. ACS cannot be held responsible for errors or consequences arising from the use of information contained in these “Just Accepted” manuscripts.

is published by the American Chemical Society. 1155 Sixteenth Street N.W.,
Washington, DC 20036

Published by American Chemical Society. Copyright © American Chemical Society. However, no copyright claim is made to original U.S. Government works, or works produced by employees of any Commonwealth realm Crown government in the course of their duties.

Remarkable Structural Diversity between Zr/Hf and Rare-Earth MOFs via Ligand Functionalization and the Discovery of Unique (4, 8)-c and (4, 12)-connected Frameworks

Giasemi K. Angeli[§], Danai Batzavali[§], Katerina Mavronassou[§], Constantinos Tsangarakis[§], Tobias Stuerzer[‡], Holger Ott[‡] and Pantelis N. Trikalitis[§,*]

[§] Department of Chemistry, University of Crete, Voutes 71003 Heraklion, Greece; [‡] Bruker AXS GmbH, Ostliche Rheinbruckenstr 49, D-76187 Karlsruhe, Germany

---

ABSTRACT: Ligand modification in MOFs provides great opportunities not only for the development of functional materials with new or enhanced properties but also for the discovery of novel structures. We report here that a sulfone functionalized tetrahedral carboxylate-based ligand is capable in directing the formation of new and fascinating MOFs when combined with Zr^{4+}/Hf^{4+} and rare-earth metal cations (RE) with improved gas-sorption properties. In particular, the resulting M-**flu**-SO_2 (M: Zr, Hf) materials display a new type of the augmented **flu**-a net which is different compared to the **flu**-a framework formed by the non-functionalized tetrahedral ligand. In terms of properties, a remarkable increase in the CO_2 uptake is observed reaching 76.6 % and 61.6 % at 273 K and 298 K and 1 bar, respectively. When combined with RE's, the sulfone modified linker affords novel MOFs, RE-**hpt**-MOF-1 (RE: Y^{3+}, Ho^{3+}, Er^{3+}), displaying a fascinating (4, 12)-coordinated **hpt** net, based on nonanuclear $[RE_9(\mu_3\text{-}O)_2(\mu_3\text{-}OH)_{12}(\text{-}COO)_{12}]$ clusters that serve as hexagonal prismatic building blocks. In the absence of the sulfone groups, we discovered that the tetrahedral linker directs the formation of new RE-MOFs, RE-**ken**-MOF-1 (RE: Y^{3+}, Ho^{3+}, Er^{3+}, Yb^{3+}), displaying an unprecedented (4, 8)-coordinated **ken** net based on nonanuclear RE_9-clusters, serving as bicapped trigonal prismatic building units. Successful activation of the representative member Y-**ken**-MOF-1 reveal a high BET surface area and total pore volume reaching 2621 $m^2\ g^{-1}$ and 0.95 $cm^3\ g^{-1}$, respectively. These values are the highest among all RE MOFs based on nonanuclear clusters and one of the highest in the entire RE family of MOFs. The present work uncovers a unique structural diversity existing between Zr/Hf and RE-based MOFs demonstrating the crucial role of linker design. In addition, the discovery of the new RE-**hpt**- MOF-1 and RE-**ken**-MOF-1 families of MOFs, highlights the great opportunities existing in RE-MOFs in terms of structural diversity that could lead to novel materials with new properties.

INTRODUCTION

The chemistry of metal-organic frameworks (MOFs) has been enormously expanded during the last decade and unique materials with remarkable structures and diverse properties have been discovered.[1-7] The systematic exploration and the discovery of novel MOFs using diverse organic linkers and metal clusters was greatly accelerated using the reticular chemistry concept based on well-defined building blocks.[8-12]

The concept of building blocks in MOFs applies to both the organic and inorganic parts of a given structure. However, from a design point of view, it is important to note that in the vast majority, the inorganic building blocks are formed in-situ during MOF synthesis, under specific reaction conditions.[10, 13, 14] This may impart noticeable limitations in MOF syntheses, because the particular synthetic conditions that lead to the formation of a specific inorganic cluster or secondary building block (SBU) need to be identified. On the other hand, the organic linker could be considered, to an extent, as a true building block because it maintains its integrity throughout the reaction. However, in many cases of MOFs based on poly-aromatic carboxylate linkers, a significant deformation of the ligand is observed compared to its free state, indicating that these are not rigid and robust building blocks.[15, 16] In other words, frequently in MOFs, the organic linker adjusts its geometrical characteristics, including bending and torsion angles of adjacent rings as well as the relative positioning of the coordinating groups, in order to fit into a particular structure.[17, 18] It is anticipated that for a given structure, there is a limit in the degree of ligand deformation beyond of which this structure will not be possible to form due to the associated increased energetics.[19] In cases where the inorganic building block can accommodate various connectivities, as in the case of Zr_6O_8 cluster, the system may find other stable configurations to form, resulting in very different MOFs.[17] In fact, the rational design of geometrical modified or de-symmetrized ligands and their use in exploratory MOF synthesis is an excellent tool towards the discovery of novel zirconium and rare-earth (RE)-based structures with important properties.[20-25]

Along the above lines, ligand functionalization has been applied as a strategy not only to impart new properties or enhance existing ones in MOFs[26], but also to alter the symmetry and geometry of an organic ligand, providing in this way further opportunities towards the discovery of new structures.[17, 23, 25, 27]

In the present work, we designed and synthesized the sulfone ($\text{-}SO_2$) functionalized derivative of the tetrahedral ligand 4',4'',4''',4''''-methanetetrayltetrabiphenyl-4-carboxylic acid (H_4MTBC), denoted here as $H_4MTBC\text{-}SO_2$, as a novel de-symmetrized building block towards the reticular synthesis of new Zr/Hf and RE MOFs, with enhanced gas sorption

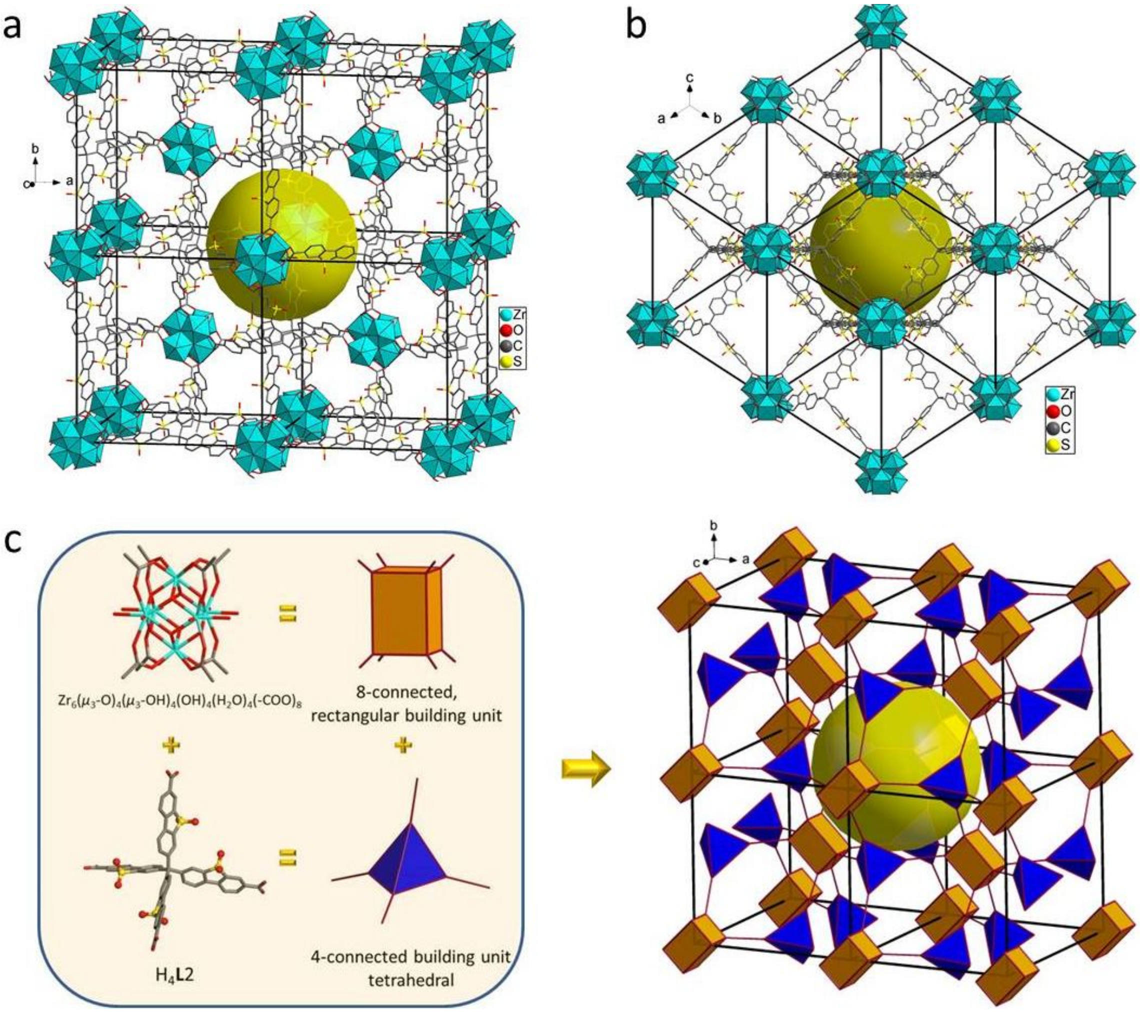

Figure 1. The structure of Zr-**flu**-SO_2 looking slightly off the c-axis (a) and along the [111] direction (b). (c) The resulting **flu**-a net formed by the 8-c inorganic and 4-c organic SBUs. The sphere highlights the pore space.

properties. We and others have demonstrated that the presence of the polar $–SO_2$ groups in MOFs increases the interaction with polar gases such as CO_2, resulting in a significantly enhanced uptake and selectivity.[28-32] The new H_4MTBC-SO_2 linker contains four $–SO_2$ polar groups, each of which is inserted through the formation of a five member ring in each of the four biphenyl arms of the parent ligand (Figure 1c). The formation of the five-member ring results in a reduction of ligand flexibility because adjacent aromatic rings cannot rotate and also, in a significant bending of each arm (the angle between the central C-sp^3 and the carbon atom of the carboxylate group is ~160°), leading to a reduction of the ligand symmetry from T_d to S_4.

The parent non-functionalized ligand, H_4MTBC, has been reported to form the augmented fluorite-type structure (**flu**-a) with both Zr_6O_8 and Hf_6O_8 clusters, however with a significant deformation, displaying D_{2d} symmetry.[33] Therefore, in addition to the effect of $–SO_2$ groups in the gas-sorption properties, an important question is whether or not H_4MTBC-SO_2 being more rigid and with different symmetry is capable of forming isostructural **flu**-a type Zr- and Hf-based MOFs. Remarkably, in both cases, highly crystalline MOFs were isolated, denoted here as M-**flu**-SO_2 (M: Zr, Hf), displaying the **flu**-a topology but these are not isostructural compared to PCN-521(Zr)/523(Hf), possessing significantly increased space group symmetry, with a different pore size and shape. In terms of properties, the presence of $–SO_2$ groups was found to greatly enhance the CO_2 uptake.

The successful syntheses of M-**flu**-SO_2 (M: Zr, Hf) MOFs prompted us to explore the construction of RE-MOFs based on the analogous hexanuclear $RE_6(\mu_3\text{-}OH)_8$ clusters and H_4MTBC-SO_2 ligand. Remarkably, we discovered an unprecedented family of (4, 12)-connected RE-MOFs, denoted here as RE-**hpt**-MOF-1, based on 12-connected nonanuclear clusters, $[RE_9(\mu_3\text{-}O)_4(\mu_3\text{-}OH)_{12}]$, displaying the novel **hpt** topology. For comparison purposes, we explored the synthesis of RE-MOFs using the non-functionalized ligand H_4MTBC and to a great surprise the new MOFs, denoted as RE-**ken**-MOF-1, display a novel (4, 8)-connected structure with the unique **ken** topology based on an unprecedented 8-connected, bicapped trigonal prismatic nonanuclear cluster. Representative members from each RE-MOF families have been activated and selected gas-sorption properties are presented and discussed.

RESULTS AND DISCUSSION

The solvothermal reaction between $ZrCl_4$ and H_4MTBC-SO_2 (H_4**L2**) in *N,N′*-dimethylformamide (DMF) at 120 °C for 12 h in the presence of benzoic acid acting as modulator, resulted in the formation of high quality octahedral shaped,

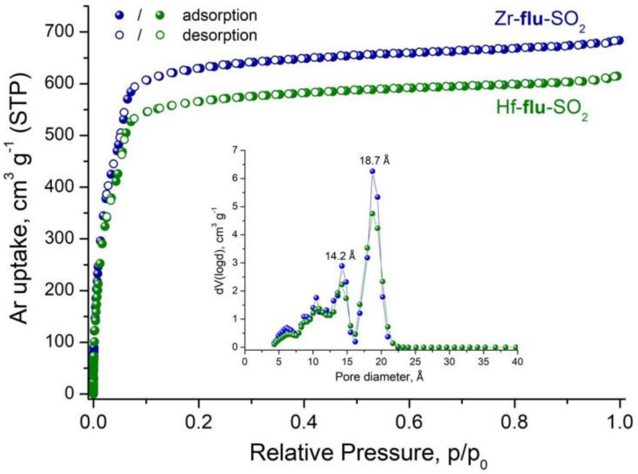

Figure 2. Argon sorption isotherms recorded at 87 K and the corresponding DFT pore size distribution curves for Zr-**flu**-SO$_2$ (blue data) and Hf-**flu**-SO$_2$ (green data).

yellowish crystals suitable for single-crystal X-ray diffraction (SCXRD) analysis (see SI). Accordingly, the material Zr-**flu**-SO$_2$ crystallizes in the tetragonal space group $P4_2/mnm$ with lattice parameters a = b = 24.6334(16) Å, c = 29.830(2) Å, V = 18101.(3) Å^3. The structure consists of 8-connected $[Zr_6(\mu_3\text{-}O)_4(\mu_3\text{-}OH)_4]^{12-}$ clusters linked together by 4-connected sulfone **L2**$^{4-}$ ligands, resulting in a 3D (4, 8)-connected framework displaying the **flu**-a topology, with an overall charge balanced chemical formula, $Zr_6(\mu_3\text{-}O)_4(\mu_3\text{-}OH)_4(OH)_4(H_2O)_4(\mathbf{L2})_2$ (Figure 1). Phase purity was confirmed by comparing the experiment powder X-ray diffraction (PXRD) pattern with that calculated from the single crystal structure (Figure S15).

In MOFs, for a given net based on a particular inorganic building block, in this case the **flu**-a net based on Zr$_6$-clusters (D_{4h} symmetry), the ligand needs to meet specific geometric requirements.[10, 12] Accordingly, as reported in PCN-521, the formation of this particular **flu**-a net requires a significant distortion of the ligand conformation and in particular, from T_d becomes D_{2d} with angles 86.8° and 122° and at the same time, adjacent phenyl rings are rotated 41.768° from each other to meet the directionality of the 8-connected Zr$_6$-clusters (Figure S14).[33] In marked contrast, in Zr-**flu**-SO$_2$ the geometric characteristics of the sulfone ligand are very different from the ligand in PCN-521 (Figure S14). In particular, adjacent phenyl rings are now locked in same plane due to the formation of a five member ring upon insertion of the sulfone group and for the same reason, each arm is highly bended with the angle between the central C-sp^3 and the carbon atom of the carboxylate group reduced from 180° to 164.7°. Furthermore, the angles between adjacent arms are 106.26° and 116.10°, indicating a significantly less distortion, compared to the ligand in PCN-521 (Figure S14). Therefore, it is quite remarkable that the sulfone functionalized linker analogue, H$_4$**L2**, is still capable in forming the **flu**-a net and in fact, with a significantly increased symmetry compared to PCN-521 ($P4_2/mnm$ vs $I4/m$) and in addition, with a very different unit cell size, pore shape and size, as we describe below. Looking carefully the crystal structures of Zr-**flu**-SO$_2$ and PCN-521, this is achieved by changing the relative positioning of the Zr$_6$-clusters (Figure S10). In particular, in the unit cell of Zr-**flu**-SO$_2$ the central Zr$_6$-cluster is rotated by 90° relative to those at the corners, where in PCN-521 all clusters have the same relative positioning (Figure S10). Therefore, Zr-**flu**-SO$_2$ represents a new type of (4, 8)-connected **flu**-a network. This kind of polymorphism in MOFs is important because each member provides distinct post synthetic functionalization opportunities (linker and/or functional group insertion) due to the different orientation of their inorganic SBU's, as in the case of PCN-700[34] and Zr-bcu-azo33.[35]

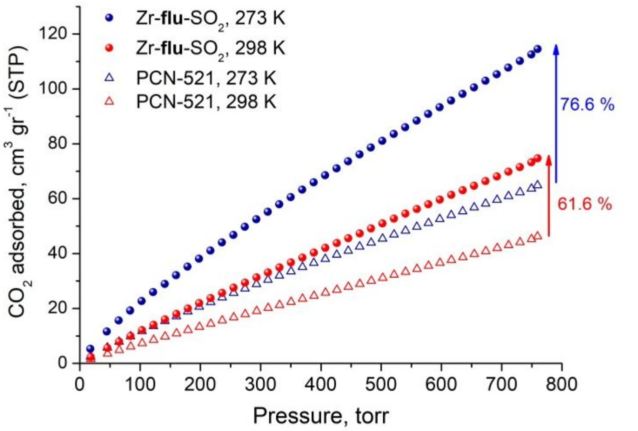

Figure 3. Carbon dioxide adsorption isotherms of Zr-**flu**-SO$_2$ and PCN-521 at the indicated temperatures up to 1 bar.

To exclude the possibility of a potential solvent effect in the formation of the different **flu**-a net types between Zr-**flu**-SO$_2$ and PCN-521, given that the former synthesized in DMF while the later in DEF (*N,N'*-diethylformamide), we attempted the synthesis of Zr-**flu**-SO$_2$ in DEF instead of DMF. The results show that Zr-**flu**-SO$_2$ is also formed however, as a powder-like solid with a poor crystallinity as confirmed by PXRD (Figure S15), indicating that the formation of the new type of **flu**-a net observed in Zr-**flu**-SO$_2$ is associated with the sulfone functionalized tetrahedral linker (H$_4$**L2**).

The unit cell volume of Zr-**flu**-SO$_2$ shows a 7.8 % increase compared to PCN-521, with a 78 % solvent accessible volume calculated by PLATON, which is almost identical to PCN-521 (78.5%).[33] The fact that the accessible solvent volume is not reduced, despite the presence of sulfone functional groups, is very interesting because both Zr-**flu**-SO$_2$ and PCN-521 are made of similar in size building blocks displaying the same (4, 8)-connectivity and attributed to the pore geometry of Zr-**flu**-SO$_2$ and the fact that the unit cell volume is increased by 7.8 % compared to PCN-521. Accordingly, the structure contains large polyhedral cavities that are significantly more regular and wider than that in PCN-521, in which an ellipsoid of approximately 14 x 19 Å can fit (Figure 1 and S9). These cavities are interconnected through smaller rhombic shaped windows of approximately 8 x 8 Å, which along the *c*-axis are decorated with sulfone groups, creating a 3D pore system that was found accessible, as confirmed experimentally by accurate microporous analysis using Ar at 87 K and described below (Figure 1).

The material is stable in H$_2$O as well as in acidic (pH 1) and basic aqueous solutions (pH 10) and in common organic solvents including acetone, CH$_3$CN and CH$_2$Cl$_2$, as confirmed by PXRD (Figures S16 and S17). Activation of Zr-**flu**-SO$_2$ was successfully achieved by applying a straightforward procedure using acetone or dichloromethane as a volatile solvent to exchange the original guest molecules followed by overnight drying under vacuum at room temperature (see SI).

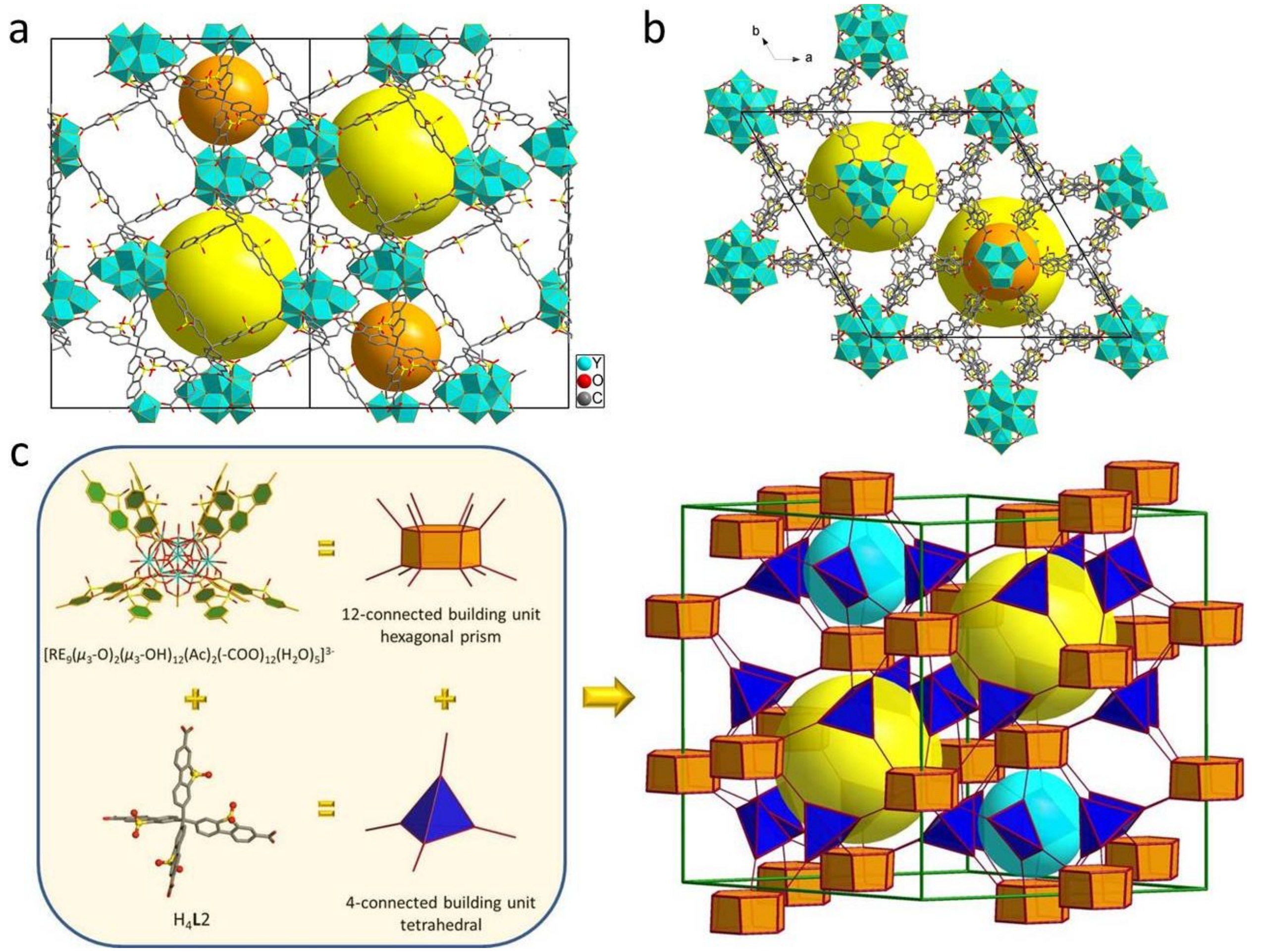

Figure 4. The structure of Y-**hpt**-MOF-1 looking down the [110] crystallographic direction (a) and the c-axis (b). (c) The novel **hpt**-a net formed by the 12-c inorganic and 4-c organic SBUs. The spheres highlight the pore space.

The complete removal of all solvent molecules was confirmed by ^{1}H NMR on a digested, activated sample (Figure S71). This is also confirmed by thermogravimetric analysis (TGA) where the material is stable up to 450 ^{o}C (Figure S74). Argon sorption isotherm recorded at 87 K confirmed the permanent porosity of Zr-**flu**-SO_2, showing a steep uptake at low relative pressures and in addition, a clearly visible condensation step occurring between 0.05 – 0.1 p/p_o, indicating the presence of small mesopores, in agreement with the crystallographic data (Figure 2). Notably, this is contrast to PCN-521 where no condensation step is visible in the corresponding isotherm indicating that the accessible pores are smaller compared to Zr-**flu**-SO_2.[33] The pore size distribution curve calculated using Non-Local Density Functional Theory (NLDFT) after a successful fitting of the Ar adsorption isotherm data using a suitable NLDFT kernel, shows two main peaks centered at 14.2 Å and 18.7 Å, in full agreement with the crystallographic data (Figure 2). The BET surface area, calculated in the pressure range 0.01-0.05 p/p_o (below the condensation step) using consistency criteria, is 2187 m^2 g^{-1} (Figure S30) while the total pore volume at 0.99 p/p_o is 0.87 cm^3 g^{-1}. The latter is close to PCN-521 (1.1 cm^3 g^{-1}), however the surface area in Zr-**flu**-SO_2 is lower due to the presence of the small mesopores.

The large accessible pore volume in Zr-**flu**-SO_2 in combination with the polarizing sulfone groups, prompted us to investigate its CO_2 adsorption properties. For comparison purposes we synthesized and successfully activated PCN-521, for which its CO_2 adsorption properties have not been reported. The corresponding CO_2 adsorption isotherms for both MOFs recorded at 273 K and 298 K shown in Figure 3, reveal a remarkable 76.6 % increase of CO_2 uptake in Zr-**flu**-SO_2 at 273 K and 1 bar, compared to PCN-521, reaching 114.5 cm^3 g^{-1} (5.11 mmol g^{-1}). At 298 K the corresponding increase is 61.6 %, reaching 74.7 cm^3 g^{-1} (3.34 mmol g^{-1}). The calculated isosteric heat of adsorption at zero coverage (Q_{st}^0) using a virial type equation is 21.8 kJ mol^{-1} and 15 kJ mol^{-1} for Zr-**flu**-SO_2 and PCN-521, respectively (Figure S41-S43, S58-S61).

The observed 45 % increase in Q_{st}^0, attributed to the polar –SO_2 groups in Zr-**flu**-SO_2, correlates well with our previously reported ab-initio calculations on a biphenyl-dicarboxylate linker, revealing that the increase in CO_2 binding strength due to the insertion of a –SO_2 group is approximately 30 %.[30] The observed Q_{st}^0 in Zr-**flu**-SO_2 is lower compared to that reported for the sulfone functionalized Zr-UiO-67 (26.5 kJ mol^{-1}) presumably due to the increased pore size in Zr-**flu**-SO_2 causing a reduction in the overlapping potential between opposite walls that in turns, reduce the CO_2-framework interactions.[30]

The isostructural Hf-**flu**-SO_2 was successfully synthesized in a single-crystal form and fully characterized (see SI). This material is also stable in H_2O as well as in acidic (pH 1) and basic aqueous solutions (pH 10) and in common organic solvents including acetone and CH_2Cl_2, as confirmed by PXRD (Figures S18 and S19). The corresponding Ar isotherm recorded at 87 K on an activated sample displays the same shape observed in Zr-**flu**-SO_2 showing a distinct condensation step (Figure 2). The corresponding NLDFT pore distribution is identical to the Zr-analogue (Figure 2). The BET surface area is 1895 m^2 g^{-1} and the total pore volume at 0.99 p/p_o is 0.78 cm^3 g^{-1} (Figures 1 and S32). The corresponding CO_2 isotherms recorded at 273 K and 298 K at 1 bar, reveal a high uptake reaching 85.1 cm^3 g^{-1} and 49.3 cm^3 g^{-1} respectively, with a Q_{st}^0 of 24 kJ mol^{-1} (Figure S44-S46). The increased Q_{st}^0 in Hf-**flu**-SO_2 as compared to Zr-**flu**-SO_2 could be attributed to the more acidic nature of the Hf_6-cluster, as it has been reported for other MOFs including NUS-6(Zr/Hf)[36] and VPI-100(Zr/Hf).[37] The observed reduced gravimetric BET surface area and CO_2 uptake is due to fact that Hf-**flu**-SO_2 is heavier than Zr-**flu**-SO_2.

For both Zr-**flu**-SO_2 and Hf-**flu**-SO_2 solids, in addition to CO_2, we measured the corresponding CH_4 sorption isotherms, from which the Q_{st}^0 and IAST CO_2/CH_4 selectivity were calculated (Figure S49-51, S53-55). Accordingly, the Q_{st}^0 value is 16 kJ mol^{-1} and 22 kJ mol^{-1} for Zr-**flu**-SO_2 and Hf-**flu**-SO_2 respectively, while the corresponding CO_2/CH_4 selectivity at 273 K and 298 K using the IAST methodology for a 5/95 molar mixture is 13.1/9.0 and 9.5/8.5 (Figure S56-57). Notably, in the case of Zr-**flu**-SO_2, the observed CO_2/CH_4 selectivity is higher compared to the sulfone functionalized Zr-UiO-67 (9.8/6.8), recorded under the same experimental conditions.[30]

The successful synthesis of M-**flu**-SO_2 (M: Zr, Hf) MOFs prompted us to investigate the synthesis of the corresponding rare-earth (RE) analogues, given the existence of the hexanuclear $[RE_6(\mu_3\text{-}OH)_8]^{10+}$ clusters.[38] The synthesis protocol was modified because the formation of RE-clusters in most cases requires the use of 2-fluorobenzoic acid (2-FBA) as modulator. However, in our case we found that a mixed modulator system, using also an excess of acetic acid, is crucial in obtaining high quality crystalline materials (see SI). Accordingly, solvothermal reactions in DMF between $RE(NO_3)_3 \cdot 6H_2O$ (RE: Y^{3+}, Ho^{3+} and Er^{3+}) and H_4**L2** in the presence of excess acetic acid and 2-FBA, afforded high quality polyhedral shaped single crystals. Based on SCXRD (Table S4-S6) and PXRD (Figure S20) analyses, these materials are isostructural and therefore only the structure of the Yttrium analogue is described below.

The material, denoted here as Y-**hpt**-MOF-1, crystallizes in the hexagonal system, space group $R\text{-}3m$, with unit cell, a = b = 39.5393(14) Å, c = 48.8586(19) Å, V = 66150 (5) $Å^3$. The structure consists of ordered 12-connected nonanuclear clusters, $[Y_9(\mu_3\text{-}O)_2(\mu_3\text{-}OH)_{12}(\text{-}COO)_{12}]$, linked together by 4-connected sulfone $\mathbf{L2}^{4-}$ ligands, resulting in a novel 3D (4, 12)-connected structure with an overall chemical formula, $[(CH_3)_2NH_2]_3[Y_9(\mu_3\text{-}O)_2(\mu_3\text{-}OH)_{12}(Ac)_2(H_2O)_3(\mathbf{L2})_3]$ (Figure 4). In addition to charge balance considerations, the presence of counterions was confirmed in a sodium exchanged analogue using a SEM/EDS, where the Na:RE was found to be very close to 1:3 as expected (Figure S28-S29 and Table S9). Phase purity was confirmed by comparing the experimental PXRD pattern with that calculated from the single crystal structure (Figure S20). Topological analysis of the obtained crystal structure revealed a new fascinating topology, denoted here as **hpt**, where the nonanuclear cluster serves as a 12-c hexagonal prismatic building block (double six-membered ring, d6R) and the sulfone linker as a 4-c tetrahedral node, forming an unprecedented (4, 12)-c net with a point symbol of $\{4^{33}.6^{30}.8^3\}\{4^6\}_3$ as determined by ToposPro[39] (Figure 4). To the best of our knowledge, the novel RE-**hpt**-MOF-1 (RE: Y^{3+}, Er^{3+}, Ho^{3+}) materials represent the first examples in which the 12-c d6R nonanuclear $[RE_9(\mu_3\text{-}O)_2(\mu_3\text{-}OH)_{12}]^{11-}$ clusters are combined with a 4-c rigid tetrahedral linker. Interestingly, looking at the top and the bottom of the nonanuclear cluster, the dihedral angles of the coordinated carboxylate groups are different and from one side is 158.2° while from the other is 173.3° (Figure S11). This particular connectivity of the d6R clusters results in the formation of two different polyhedral cavities in Y-**hpt**-MOF-1 stacked one on the top of the other, along the c-axis (Figure 4 and S11). In particular, the large cavity consists of 8 d6R clusters and 12 linkers and has an ellipsoid shape of approximately 20x30 Å, taking the distances from opposite clusters, while the smaller one, with a more symmetric rhombic shape of 10x12 Å cavity is made of two 2 d6R clusters and 6 linkers (Figure S11). These cavities are interconnected via rectangular windows forming a complex 3D pore system (Figure 4). Regarding the geometric configuration of the sulfone linker, this is more distorted compared to M-**flu**-SO_2 (M: Zr, Hf) MOFs with the angles between adjacent arms found in the range 95.84°-131.1° (Figure S14).

Nitrogen sorption measurements on an activated Y-**hpt**-MOF-1 revealed a type-I isotherm with a total pore volume of 0.25 cm^3 g^{-1} at 0.99 p/p_o which is lower compared to the calculated value from the single crystal structure (1.1 cm^3 g^{-1}), indicating a partial activation (Figure S35). This is also reflected in the pore size distribution curve obtained from an Argon sorption isotherm at 87 K, were a main peak centered at around 6 Å is observed (Figure S36 and S37). However, CO_2 adsorption measurements at 273 K, 283 K and 298 K revealed a high uptake, reaching 119.8 cm^3 g^{-1}, 109.6 cm^3 g^{-1} and 96.5 cm^3 g^{-1} respectively at 1 bar, which is higher compared to Zr-**flu**-SO_2 at the same conditions (114.5 cm^3 g^{-1} and 74.7 cm^3 g^{-1} at 273 K and 298 K) (Figure S62). The corresponding isosteric heat of adsorption at zero coverage is 22.2 kJ mol^{-1} which is higher compared to Zr-**flu**-SO_2 (21.8 kJ mol^{-1}) and supports the observed higher CO_2 uptake of the former (Figure S64). The enhanced CO_2 uptake in Y-**hpt**-MOF-1 is attributed to the increased density of the polar $-SO_2$ groups by 23.1 % (based on the number of $-SO_2$ groups per unit cell volume) and the ionic nature of the material that increases the CO_2-framework interactions, presumably via a dipole-induce dipole mechanism.

An important question is whether or not the formation of the fascinating structure of RE-**hpt**-MOF-1 is associated with the sulfone functionalized linker displaying the S_4 symmetry. To answer this question, we targeted the synthesis of RE-MOFs based on the tetrahedral non-functionalized linker H_4MTBC (H_4**L**). Accordingly, using $Y(NO_3)_3 \cdot 6H_2O$ and following a very similar synthetic procedure but adjusting the molar ratio of the modulators (acetic acid and 2-FBA), high quality hexagonal crystals were obtained (Figure S8). Under the same reaction conditions, we obtained isostructural analogues as confirmed by SXCRD and PXRD, denoted here as RE-**ken**-MOF-1 (RE: Y^{3+}, Ho^{3+}, Er^{3+}, Yb^{3+}) and below the structure of Y-**ken**-MOF-1 is described in detail (Figure S24).

Remarkably, SCXRD analysis of Y-**ken**-MOF-1 revealed the formation of a novel structure that crystallizes in the trigonal system, space group P-31c, with unit cell a = b = 25.4495(5) Å, c = 39.5438(8) Å, V = 22180.3 (10) Å^3 made of 8-connected nonanuclear clusters, [$Y_9(\mu_3\text{-}O)_2(\mu_3\text{-}OH)_{12}(\text{-}COO)_8$], bridged together by 4-c tetrahedral linkers that preserves their T_d symmetry (Figure 5 and Table S7). In particular, eight carboxylate groups from eight different 4-c tetrahedral linkers are coordinated to Y$_9$-clusters in a bicapped trigonal prismatic fashion (Figure 5). Interestingly, along the c-axis, pairs of opposite linkers are formed and connect six Y$_9$-clusters in a regular trigonal prismatic arrangement (Figure 5 and S13). Each Y$_9$-cluster is connected to twelve other Y$_9$-clusters, six in equatorial position via three pairs of linkers and six more, three on the top and three on the bottom, via two more linkers (Figure S13). This is an unprecedented connectivity and the analysis using ToposPro[39] revealed the formation of the **ken** topology as registered in the RCSR database,[40] where the 8-c Y$_9$-clusters serve as bicapped trigonal prismatic building blocks bridged via the 4-c T_d linkers to form a unique (4, 8)-c net with point symbol $\{4^6\}_2\{4^9.6^{18}.8\}$ (Figure 5). In the crystal structure the Y$_9$-clusters are found disordered over two positions as it has been observed in other cases of RE-MOFs based on nonanuclear clusters, including Y-**kce**-MOF-1[41], Y-**shp**-MOF-1[42] and Y-**shp**-MOF-5[43] (Figure S12). Careful analysis using ^{1}H NMR in an acid digested material and SEM/EDS in a sodium exchanged sample, revealed that the framework is neutral with a charged balanced chemical formula, $Y_9(\mu_3\text{-}O)_2(\mu_3\text{-}OH)_{12}(OH)_2(H_2O)_{11}\mathbf{L}_2$ (Figure S27, S73 and Table S8).

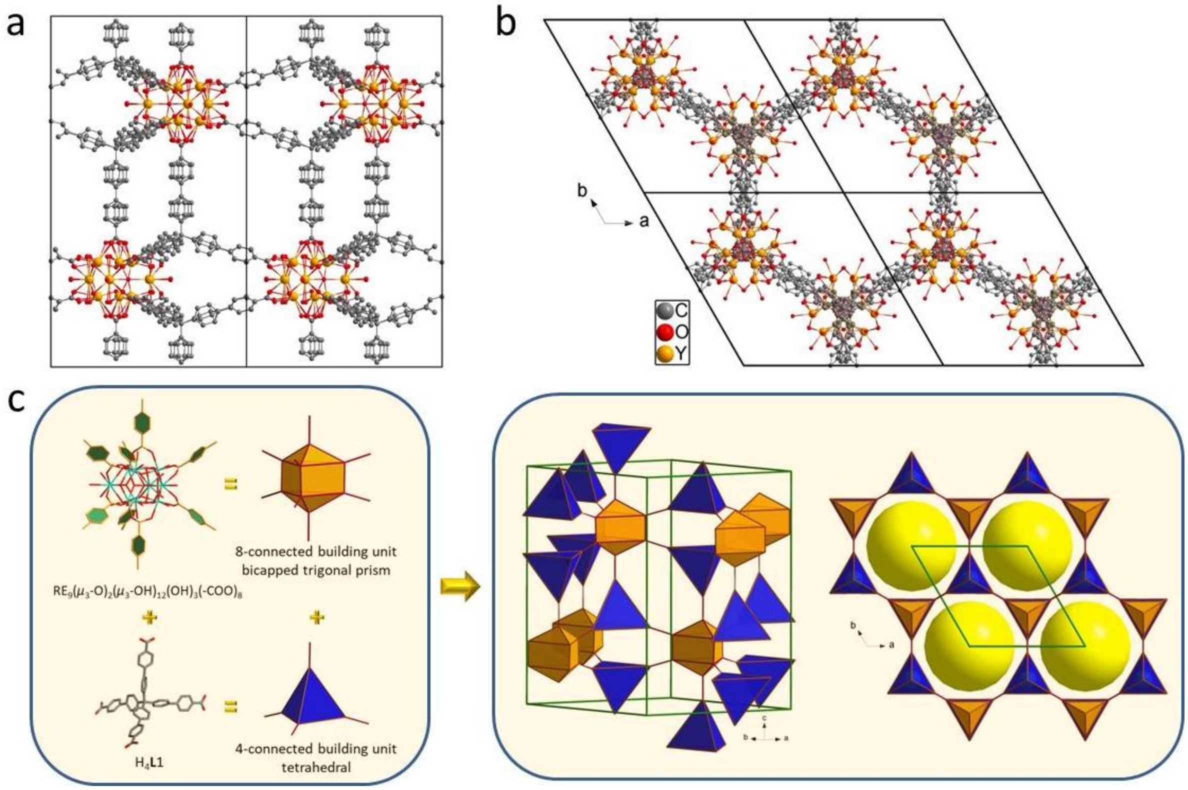

Figure 5. The structure of Y-**ken**-MOF-1 looking down the b-axis (a) and the c-axis (b). (c) The novel **ken**-a net formed by the 8-c inorganic and 4-c organic SBUs. The yellow spheres highlight the pore space.

The structure of Y-**ken**-MOF-1 contains 1D hexagonal pores of approximately 15 Å in diameter running along the c-axis and these are connected to each other via 9x9 Å rhombic shaped windows, running along the a- and b-axis, creating an interconnected 3D pore system (Figure 5). The solvent accessible volume calculated by PLATON is 75 % and found to be accessible by gas sorption measurements on an activated material. In particular, Argon sorption measurements at 87 K revealed a fully reversible type I isotherm displaying a high uptake, reaching 744 cm^3 g^{-1} at p/p$_0$ 0.98, which corresponds to a total pore volume of 0.95 cm^3 g^{-1} (Figure 6). It is noted that the experimental total pore volume is half of what is expected from the single crystal structure (1.86 cm^3 g^{-1}), indicating a partial activation. The fact that the experimental pore size distribution (PSD) matches very well the expected value**s** from the single crystal structure, as we describe below, suggests that some of the pores in Y-**ken**-MOF-1 are inaccessible presumably due to the presence of residual ligand and/or metal oxide clusters. This proposition is supported by thermogravimetric analysis (TGA) and infrared spectroscopy (Figure S75 and S76)**.** The BET equation was applied successfully in the p/p$_o$ range 0.015-0.047 using consistency criteria, revealing a high surface area of 2621 m^2 g^{-1}

(Langmuir 2879 m^2 g^{-1}) (Figure S38). The observed BET surface area and total pore volume of Y-**ken**-MOF-1 is the highest among all reported MOFs based on nonanuclear RE$_9$-clusters including Y-**kex**-MOF-1[41] (1580 m^2 g^{-1}, 0.84 cm^3 g^{-1}), Y-**shp**-MOF-1[42] (2200 m^2 g^{-1}, 0.84 cm^3 g^{-1}), Y-**pek**-MOF-1[44] (1608 m^2 g^{-1}, 0.58 cm^3 g^{-1}), Y-**aea**-MOF-1[44] (1435 m^2 g^{-1}, 0.49 cm^3 g^{-1}) and among the highest in the entire RE-based family of MOFs[25, 27, 45-47] (Table S**10**). The PSD curve obtained by applying a suitable NLDFT kernel shows two peaks at 9.5 Å and 14 Å, very close to the crystallographic pore sizes (Figure S**40**). The gas sorption properties of Y-**ken**-MOF-1 were further explored by recording CH_4, CO_2 and Xe sorption isotherms at different temperatures. The CH_4 isotherm recorded at its boiling point (112 K) resembles that of Ar at 87 K, revealing a total pore volume of 0.95 cm^3 g^{-1}, in full agreement with the Ar data (Figure 6). Interestingly, the CO_2 isotherm at 195 K shows an almost linear increase in the uptake up to 250 torr forming thereafter a plateau, reaching 563.2 cm^3 g^{-1} at 0.99 p/p$_0$ (total pore volume, 0.88 cm^3 g^{-1}) and attributed to the particular pore size and structure of Y-**ken**-MOF-1 (Figure 6). The isosteric heat of adsorption was calculated using the CO_2 isotherms at 273 K (uptake 85.1 cm^3 g^{-1} at 1 bar) and 298 K (uptake 37.8 cm^3 g^{-1} at 1 bar) and found to be 20.3 kJ mol^{-1} at zero coverage (Q_{st}^0) and remains constant as a function of surface coverage, indicating an energetically uniform pore environment (Figure S65-S67). The lower Q_{st}^0 compare to the Y-**hpt**-MOF-1 (22.2 kJ mol^{-1}) is consistent with the observed lower CO_2 uptake (Figure S65).

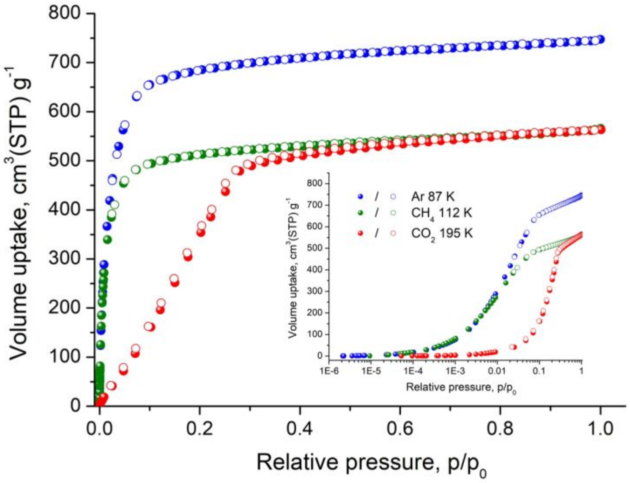

Figure 6. Ar (blue), CH_4 (green) and CO_2 (red) sorption isotherms in linear and semi logarithmic scale (inset) of Y-**ken**-MOF-1 recorder at their boiling point temperature. Closed symbols represent adsorption and open symbols desorption.

Finally, because Xe storage[48] in porous materials is considered an important application and the combination of high surface area and high pore volume plays a key role, we examined the Xe adsorption properties of Y-**ken**-MOF-1 at different temperatures. The corresponding isotherms recorded at 240 K, 273 K and 298 K reveal an uptake of 166.4 cm^3 g^{-1} (7.4 mmol g^{-1}), 88.8 cm^3 g^{-1} (3.9 mmol g^{-1}) and 39.8 cm^3 g^{-1} (1.8 mmol g^{-1}) respectively, with a Q_{st}^0 of 22.3 kJ mol^{-1} (Figure S68-S70). Although these are moderate values compared to the state-of-the-art Xe storage MOFs displaying a high density of unsaturated metal sites[48], the observed uptake is very similar to that reported for Y-**csq**-MOF-1 exhibiting a similar 1D hexagonal pore system (3.37 and 1.94 mmol g^{-1} at 273 K and 298 K, respectively).[49] However, Q_{st}^0 is significantly reduced in Y-**ken**-MOF-1 (22.3 vs 33.8 kJ mol^{-1} in Y-**csq**-MOF-1), which is preferable for Xe storage applications, due to the associated reduced energy demand for Xe delivery.

CONCLUSIONS

In conclusion, we report a rare case where ligand functionalization has a remarkable effect in the final structure when combined with Zr/Hf and RE-metal cations and led to the discovery of novel MOFs. The sulfone functionalized tetrahedral ligand $H_4MTBC\text{-}SO_2$ with Zr/Hf affords new MOFs, M-**flu**-SO$_2$ (M: Zr, Hf), based on the corresponding hexanuclear clusters with **flu**-a topology which are not isostructural with the analogous MOFs (PCN-521 and PCN-523) based on the non-functionalized tetrahedral ligand, displaying a different type of the **flu**-a net. Highly unusual is the fact the M-**flu**-SO$_2$ (M: Zr, Hf) display larger pores, in the mesopore range, compared to PCN-521/523 despite the presence of $-SO_2$ groups. These polar groups in combination with the particular pore structure results in a remarkable enhancement of CO_2 adsorption uptake in M-**flu**-SO$_2$ (M: Zr, Hf). The $H_4MTBC\text{-}SO_2$ ligand when combined with RE's afforded a novel family of MOFs based on nonanuclear RE$_9$-clusters, RE-**hpt**-MOF-1, displaying an unprecedented (4, 12)-connected network. The corresponding structure contains two different polyhedral cavities and the Y-analogue, although was partially activated, shows a higher CO_2 uptake compared to Zr-**flu**-SO$_2$ under the same conditions. Finally, in an effort to understand the role of this particular sulfone linker in directing the structure of RE-**hpt**-MOF-1, we discovered that the parent non-functionalized H_4MTBC ligand with RE's directs the formation of novel (4, 8)-connected MOFs, RE-**ken**-MOF-1. These RE-MOFs are neutral, based on a unique 8-connected nonanuclear RE$_9$-cluster that serves as a bicapped trigonal prismatic building unit and features large hexagonal channels. The Y-**ken**-MOF-1 analogue was successfully activated and shows a very high BET area and pore volume. The discovery of the new RE families of MOFs, RE-**hpt**-MOF-1 and RE-**ken**-MOF-1, demonstrates the great opportunities existing in RE-MOFs in terms of structural diversity, that could lead to novel MOFs with new properties. In particular, the structure of RE-**ken**-MOF-1 is an excellent platform for isoreticular expansion, using elongated tetrahedral linkers, towards highly porous RE-MOFs and we are currently working on this direction.

ASSOCIATED CONTENT

Experimental details, single crystal and powder XRD data, EDS, gas sorption isotherms and related calculations, NMR and TGA. This material is available free of charge via the Internet at http://pubs.acs.org.

AUTHOR INFORMATION

Corresponding Author

* ptrikal@uoc.gr

ACKNOWLEDGMENT

This research has been co-financed by the European Regional Development Fund of the European Union and Greek national funds through the Operational Program Competitiveness, Entrepreneurship and Innovation, under the call RESEARCH – CREATE – INNOVATE (project code:T1EDK-00770).

REFERENCES

(1) Furukawa, H.; Cordova, K. E.; O'Keeffe, M.; Yaghi, O. M., The Chemistry and Applications of Metal-Organic Frameworks. *Science* **2013,** *341* (6149), 974.

(2) Bennett, T. D.; Cheetham, A. K.; Fuchs, A. H.; Coudert, F.-X., Interplay between defects, disorder and flexibility in metal-organic frameworks. *Nat. Chem.* **2017,** *9* (1), 11-16.

(3) Foo, M. L.; Matsuda, R.; Kitagawa, S., Functional Hybrid Porous Coordination Polymers. *Chem. Mater.* **2014,** *26* (1), 310-322.

(4) Hendon, C. H.; Rieth, A. J.; Korzyński, M. D.; Dincă, M., Grand Challenges and Future Opportunities for Metal–Organic Frameworks. *ACS Cent. Sci.* **2017,** *3* (6), 554-563.

(5) Coudert, F.-X.; Evans, J. D., Nanoscale metamaterials: Meta-MOFs and framework materials with anomalous behavior. *Coord. Chem. Rev.* **2019,** *388*, 48-62.

(6) Ding, M. L.; Flaig, R. W.; Jiang, H. L.; Yaghi, O. M., Carbon capture and conversion using metal-organic frameworks and MOF-based materials. *Chem. Soc. Rev.* **2019,** *48* (10), 2783-2828.

(7) Zhang, L. L.; Yuan, S.; Feng, L.; Guo, B. B.; Qin, J. S.; Xu, B.; Lollar, C.; Sun, D. F.; Zhou, H. C., Pore-Environment Engineering with Multiple Metal Sites in Rare-Earth Porphyrinic Metal-Organic Frameworks. *Angew. Chem. Int. Ed.* **2018,** *57* (18), 5095-5099.

(8) Alezi, D.; Spanopoulos, I.; Tsangarakis, C.; Shkurenko, A.; Adil, K.; Belmabkhout, Y.; O'Keeffe, M.; Eddaoudi, M.; Trikalitis, P. N., Reticular Chemistry at Its Best: Directed Assembly of Hexagonal Building Units into the Awaited Metal-Organic Framework with the Intricate Polybenzene Topology, pbz-MOF. *J. Am. Chem. Soc.* **2016,** *138* (39), 12767-12770.

(9) Chen, Z.; Hanna, S. L.; Redfern, L. R.; Alezi, D.; Islamoglu, T.; Farha, O. K., Reticular chemistry in the rational synthesis of functional zirconium cluster-based MOFs. *Coord. Chem. Rev.* **2019,** *386*, 32-49.

(10) Kalmutzki, M. J.; Hanikel, N.; Yaghi, O. M., Secondary building units as the turning point in the development of the reticular chemistry of MOFs. *Sci. Adv.* **2018,** *4*, No. eaat9180.

(11) Yaghi, O. M.; O'Keeffe, M.; Ockwig, N. W.; Chae, H. K.; Eddaoudi, M.; Kim, J., Reticular synthesis and the design of new materials. *Nature* **2003,** *423* (6941), 705-714.

(12) Yaghi, O. M.; Kalmutzki, M. J.; Diercks, C. S., Introduction to Reticular Chemistry. *Wiley* **2019**.

(13) Alezi, D.; Belmabkhout, Y.; Suyetin, M.; Bhatt, P. M.; Weseliński, Ł. J.; Solovyeva, V.; Adil, K.; Spanopoulos, I.; Trikalitis, P. N.; Emwas, A.-H.; Eddaoudi, M., MOF Crystal Chemistry Paving the Way to Gas Storage Needs: Aluminum-Based soc-MOF for CH4, O2, and CO2 Storage. *J. Am. Chem. Soc.* **2015,** *137* (41), 13308-13318.

(14) Guillerm, V.; Kim, D.; Eubank, J. F.; Luebke, R.; Liu, X.; Adil, K.; Lah, M. S.; Eddaoudi, M., A supermolecular building approach for the design and construction of metal–organic frameworks. *Chem. Soc. Rev.* **2014,** *43* (16), 6141-6172.

(15) Lv, X.-L.; Yuan, S.; Xie, L.-H.; Darke, H. F.; Chen, Y.; He, T.; Dong, C.; Wang, B.; Zhang, Y.-Z.; Li, J.-R.; Zhou, H.-C., Ligand Rigidification for Enhancing the Stability of Metal–Organic Frameworks. *J. Am. Chem. Soc.* **2019,** *141* (26), 10283-10293.

(16) Zhang, X.; Frey, B. L.; Chen, Y.-S.; Zhang, J., Topology-Guided Stepwise Insertion of Three Secondary Linkers in Zirconium Metal–Organic Frameworks. *J. Am. Chem. Soc.* **2018,** *140* (24), 7710-7715.

(17) Lyu, J.; Zhang, X.; Otake, K.-i.; Wang, X.; Li, P.; Li, Z.; Chen, Z.; Zhang, Y.; Wasson, M. C.; Yang, Y.; Bai, P.; Guo, X.; Islamoglu, T.; Farha, O. K., Topology and porosity control of metal–organic frameworks through linker functionalization. *Chem. Sci.* **2019,** *10* (4), 1186-1192.

(18) Zhang, X.; Zhang, X.; Johnson, J. A.; Chen, Y.-S.; Zhang, J., Highly Porous Zirconium Metal–Organic Frameworks with β-UH3-like Topology Based on Elongated Tetrahedral Linkers. *J. Am. Chem. Soc.* **2016,** *138* (27), 8380-8383.

(19) Zhang, Y.-B.; Furukawa, H.; Ko, N.; Nie, W.; Park, H. J.; Okajima, S.; Cordova, K. E.; Deng, H.; Kim, J.; Yaghi, O. M., Introduction of Functionality, Selection of Topology, and Enhancement of Gas Adsorption in Multivariate Metal–Organic Framework-177. *J. Am. Chem. Soc.* **2015,** *137* (7), 2641-2650.

(20) Ma, J. L.; Tran, L. D.; Matzger, A. J., Toward Topology Prediction in Zr-Based Microporous Coordination Polymers: The Role of Linker Geometry and Flexibility. *Cryst. Growth Des.* **2016,** *16* (7), 4148-4153.

(21) Wang, Y.; Feng, L.; Zhang, K.; Wang, K.-Y.; Fan, W.; Wang, X.; Guo, B.; Dai, F.; Zhang, L.; Sun, D.; Zhou, H.-C., Uncovering Structural Opportunities for Zirconium Metal–Organic Frameworks via Linker Desymmetrization. *Adv. Sci.* **2019,** *6* (23), 1901855.

(22) Ortín-Rubio, B.; Ghasempour, H.; Guillerm, V.; Morsali, A.; Juanhuix, J.; Imaz, I.; Maspoch, D., Net-Clipping: An Approach to Deduce the Topology of Metal–Organic Frameworks Built with Zigzag Ligands. *J. Am. Chem. Soc.* **2020,** *142* (20), 9135-9140.

(23) Guillerm, V.; Maspoch, D., Geometry Mismatch and Reticular Chemistry: Strategies To Assemble Metal–Organic Frameworks with Non-default Topologies. *J. Am. Chem. Soc.* **2019,** *141* (42), 16517-16538.

(24) Wang, H.; Dong, X.; Lin, J.; Teat, S. J.; Jensen, S.; Cure, J.; Alexandrov, E. V.; Xia, Q.; Tan, K.; Wang, Q.; Olson, D. H.; Proserpio, D. M.; Chabal, Y. J.; Thonhauser, T.; Sun, J.; Han, Y.; Li, J., Topologically guided tuning of Zr-MOF pore structures for highly selective separation of C6 alkane isomers. *Nat. Commun.* **2018,** *9* (1), 1745.

(25) Feng, L.; Wang, Y.; Zhang, K.; Wang, K.-Y.; Fan, W.; Wang, X.; Powell, J. A.; Guo, B.; Dai, F.; Zhang, L.; Wang, R.; Sun, D.; Zhou, H.-C., Molecular Pivot-Hinge Installation to Evolve Topology in Rare-Earth Metal–Organic Frameworks. *Angew. Chem. Int. Ed.* **2019,** *58* (46), 16682-16690.

(26) Jiang, H.; Zhang, W. Q.; Kang, X.; Cao, Z. P.; Chen, X.; Liu, Y.; Cui, Y., Topology-Based Functionalization of Robust Chiral Zr-Based Metal-Organic Frameworks for Catalytic Enantioselective Hydrogenation. *J. Am. Chem. Soc.* **2020,** *142* (21), 9642-9652.

(27) Wang, Y. T.; Feng, L.; Fan, W. D.; Wang, K. Y.; Wang, X.; Wang, X. K.; Zhang, K.; Zhang, X. R.; Dai, F. N.; Sun, D. F.; Zhou, H. C., Topology Exploration in Highly Connected Rare-Earth Metal-Organic Frameworks via Continuous Hindrance Control. *J. Am. Chem. Soc.* **2019,** *141* (17), 6967-6975.

(28) Chakraborty, G.; Das, P.; Mandal, S. K., Polar Sulfone-Functionalized Oxygen-Rich Metal–Organic Frameworks for Highly Selective CO2 Capture and Sensitive Detection of Acetylacetone at ppb Level. *ACS Appl. Mater. Interfaces* **2020,** *12* (10), 11724-11736.

(29) Wang, B.; Huang, H.; Lv, X.-L.; Xie, Y.; Li, M.; Li, J.-R., Tuning CO2 Selective Adsorption over N2 and CH4 in UiO-67 Analogues through Ligand Functionalization. *Inorg. Chem.* **2014,** *53* (17), 9254-9259.

(30) Xydias, P.; Spanopoulos, I.; Klontzas, E.; Froudakis, G. E.; Trikalitis, P. N., Drastic Enhancement of the CO2 Adsorption Properties in Sulfone-Functionalized Zr- and Hf-UiO-67 MOFs with Hierarchical Mesopores. *Inorg. Chem.* **2014,** *53* (2), 679-681.

(31) Couck, S.; Liu, Y.-Y.; Leus, K.; Baron, G. V.; Van der Voort, P.; Denayer, J. F. M., Gas phase adsorption of alkanes, alkenes and aromatics on the sulfone-DUT-5 Metal Organic Framework. *Microporous Mesoporous Mater.* **2015,** *206*, 217-225.

(32) Wang, G.; Leus, K.; Couck, S.; Tack, P.; Depauw, H.; Liu, Y.-Y.; Vincze, L.; Denayer, J. F. M.; Van Der Voort, P., Enhanced gas sorption and breathing properties of the new sulfone functionalized COMOC-2 metal organic framework. *Dalton Trans.* **2016,** *45* (23), 9485-9491.

(33) Zhang, M. W.; Chen, Y. P.; Bosch, M.; Gentle, T.; Wang, K. C.; Feng, D. W.; Wang, Z. Y. U.; Zhou, H. C., Symmetry-Guided Synthesis of Highly Porous Metal-Organic Frameworks with Fluorite Topology. *Angew. Chem. Int. Ed.* **2014,** *53* (3), 815-818.

(34) Yuan, S.; Lu, W.; Chen, Y.-P.; Zhang, Q.; Liu, T.-F.; Feng, D.; Wang, X.; Qin, J.; Zhou, H.-C., Sequential Linker Installation:

Precise Placement of Functional Groups in Multivariate Metal–Organic Frameworks. *J. Am. Chem. Soc.* **2015,** *137* (9), 3177-3180.

(35) Guillerm, V.; Grancha, T.; Imaz, I.; Juanhuix, J.; Maspoch, D., Zigzag Ligands for Transversal Design in Reticular Chemistry: Unveiling New Structural Opportunities for Metal–Organic Frameworks. *J. Am. Chem. Soc.* **2018,** *140* (32), 10153-10157.

(36) Hu, Z. G.; Peng, Y. W.; Gao, Y. J.; Qian, Y. H.; Ying, S. M.; Yuan, D. Q.; Horike, S.; Ogiwara, N.; Babarao, R.; Wang, Y. X.; Yan, N.; Zhao, D., Direct Synthesis of Hierarchically Porous Metal-Organic Frameworks with High Stability and Strong Bronsted Acidity: The Decisive Role of Hafnium in Efficient and Selective Fructose Dehydration. *Chem. Mater.* **2016,** *28* (8), 2659-2667.

(37) Zhu, J.; Liu, J.; Machain, Y.; Bonnett, B.; Lin, S.; Cai, M.; Kessinger, M. C.; Usov, P. M.; Xu, W.; Senanayake, S. D.; Troya, D.; Esker, A. R.; Morris, A. J., Insights into CO2 adsorption and chemical fixation properties of VPI-100 metal–organic frameworks. *Journal of Materials Chemistry A* **2018,** *6* (44), 22195-22203.

(38) Xue, D.-X.; Cairns, A. J.; Belmabkhout, Y.; Wojtas, L.; Liu, Y.; Alkordi, M. H.; Eddaoudi, M., Tunable Rare-Earth fcu-MOFs: A Platform for Systematic Enhancement of CO2 Adsorption Energetics and Uptake. *J. Am. Chem. Soc.* **2013,** *135* (20), 7660-7667.

(39) Blatov, V. A.; Shevchenko, A. P.; Proserpio, D. M., Applied Topological Analysis of Crystal Structures with the Program Package ToposPro. *Cryst. Growth Des.* **2014,** *14* (7), 3576-3586.

(40) O'Keeffe, M.; Peskov, M. A.; Ramsden, S. J.; Yaghi, O. M., The Reticular Chemistry Structure Resource (RCSR) Database of, and Symbols for, Crystal Nets. *Acc. Chem. Res.* **2008,** *41* (12), 1782-1789.

(41) Chen, Z.; Thiam, Z.; Shkurenko, A.; Weselinski, L. J.; Adil, K.; Jiang, H.; Alezi, D.; Assen, A. H.; O'Keeffe, M.; Eddaoudi, M., Enriching the Reticular Chemistry Repertoire with Minimal Edge-Transitive Related Nets: Access to Highly Coordinated Metal–Organic Frameworks Based on Double Six-Membered Rings as Net-Coded Building Units. *J. Am. Chem. Soc.* **2019,** *141* (51), 20480-20489.

(42) Chen, Z.; Weseliński, Ł. J.; Adil, K.; Belmabkhout, Y.; Shkurenko, A.; Jiang, H.; Bhatt, P. M.; Guillerm, V.; Dauzon, E.; Xue, D.-X.; O'Keeffe, M.; Eddaoudi, M., Applying the Power of Reticular Chemistry to Finding the Missing alb-MOF Platform Based on the (6,12)-Coordinated Edge-Transitive Net. *J. Am. Chem. Soc.* **2017,** *139* (8), 3265-3274.

(43) AbdulHalim, R. G.; Bhatt, P. M.; Belmabkhout, Y.; Shkurenko, A.; Adil, K.; Barbour, L. J.; Eddaoudi, M., A Fine-Tuned Metal–Organic Framework for Autonomous Indoor Moisture Control. *J. Am. Chem. Soc.* **2017,** *139* (31), 10715-10722.

(44) Alezi, D.; Peedikakkal, A. M. P.; Weseliński, Ł. J.; Guillerm, V.; Belmabkhout, Y.; Cairns, A. J.; Chen, Z.; Wojtas, Ł.; Eddaoudi, M., Quest for Highly Connected Metal–Organic Framework Platforms: Rare-Earth Polynuclear Clusters Versatility Meets Net Topology Needs. *J. Am. Chem. Soc.* **2015,** *137* (16), 5421-5430.

(45) Luebke, R.; Belmabkhout, Y.; Weselinski, L. J.; Cairns, A. J.; Alkordi, M.; Norton, G.; Wojtas, L.; Adil, K.; Eddaoudi, M., Versatile rare earth hexanuclear clusters for the design and synthesis of highly-connected ftw-MOFs. *Chem. Sci.* **2015,** *6* (7), 4095-4102.

(46) Luo, T.-Y.; Liu, C.; Eliseeva, S. V.; Muldoon, P. F.; Petoud, S.; Rosi, N. L., Rare Earth pcu Metal–Organic Framework Platform Based on RE4(μ3-OH)4(COO)62+ Clusters: Rational Design, Directed Synthesis, and Deliberate Tuning of Excitation Wavelengths. *J. Am. Chem. Soc.* **2017,** *139* (27), 9333-9340.

(47) Li, Y.-J.; Wang, Y.-L.; Liu, Q.-Y., The Highly Connected MOFs Constructed from Nonanuclear and Trinuclear Lanthanide-Carboxylate Clusters: Selective Gas Adsorption and Luminescent pH Sensing. *Inorg. Chem.* **2017,** *56* (4), 2159-2164.

(48) Elsaidi, S. K.; Ongari, D.; Mohamed, M. H.; Xu, W.; Motkuri, R. K.; Haranczyk, M.; Thallapally, P. K., Metal Organic Frameworks for Xenon Storage Applications. *ACS Mater. Lett.* **2020,** *2* (3), 233-238.

(49) Angeli, G. K.; Sartsidou, C.; Vlachaki, S.; Spanopoulos, I.; Tsangarakis, C.; Kourtellaris, A.; Klontzas, E.; Froudakis, G. E.; Tasiopoulos, A.; Trikalitis, P. N., Reticular Chemistry and the Discovery of a New Family of Rare Earth (4, 8)-Connected Metal-Organic Frameworks with csq Topology Based on RE4(μ3-O)2(COO)8 Clusters. *ACS Appl. Mater. Interfaces* **2017,** *9* (51), 44560-44566.

Table of Contents artwork